Analytica Chimica Acta: X 6 (2020) 100059

Contents lists available at ScienceDirect

Analytica Chimica Acta: X

journal homepage: www.journals.elsevier.com/analytica-chimica-acta-x

Experimental determination of the bioluminescence resonance energy transfer (BRET) Förster distances of NanoBRET and red-shifted BRET pairs

Felix Weihs [a, *], Jian Wang [b], Kevin D.G. Pfleger [c, d, e], Helen Dacres [f]

[a] CSIRO Health & Biosecurity, Parkville, 343 Royal Parade, Melbourne, VIC, 3030, Australia
[b] CSIRO Health & Biosecurity, Canberra, ACT, 2601, Australia
[c] Harry Perkins Institute of Medical Research and Centre for Medical Research, The University of Western Australia, Nedlands, Perth, WA, 6009, Australia
[d] Australian Research Council Centre for Personalised Therapeutics Technologies, Australia
[e] Dimerix Limited, Nedlands, WA, Australia
[f] CSIRO Health & Biosecurity, Food Innovation Centre, 671 Sneydes Road, Werribee, VIC, 3030, Australia

ARTICLE INFO

Article history:
Received 5 June 2020
Received in revised form
8 August 2020
Accepted 30 August 2020
Available online 2 September 2020

Keywords:
Förster distance
Bioluminescence resonance energy transfer
NanoBRET
NanoLuc
HaloTag
G-protein coupled receptors

ABSTRACT

Bioluminescence Resonance Energy Transfer (BRET) is widely applied to study protein-protein interactions, as well as increasingly to monitor both ligand binding and molecular rearrangements. The Förster distance (R_0) describes the physical distance between the two chromophores at which 50% of the maximal energy transfer occurs and it depends on the choice of RET components. R_0 can be experimentally determined using flexible peptide linkers of known lengths to separate the two chromophores. Knowledge of the R_0 helps to inform on the choice of BRET system. For example, we have previously shown that BRET^2 exhibits the largest R_0 to date for any genetically encoded RET pair, which may be advantageous for investigating large macromolecular complexes if its issues of low and fast-decaying bioluminescence signal can be accommodated.

In this study we have determined R_0 for a range of bright and red-shifted BRET pairs, including NanoBRET with tetramethylrhodamine (TMR), non-chloro TOM (NCT), mCherry or Venus as acceptor, and BRET^6, a red-shifted BRET^2-like system. This study revealed R_0 values of 6.15 nm and 6.94 nm for NanoBRET using TMR or NCT as acceptor ligands, respectively. R_0 was 5.43 nm for NanoLuc-mCherry, 5.59 nm for NanoLuc-Venus and 5.47 nm for BRET^6. This extends the palette of available BRET Förster distances, to give researchers a better-informed choice when considering BRET systems and points towards NanoBRET with NCT as a good alternative to BRET^2 as an analysis tool for large macromolecular complexes.

1. Introduction

Bioluminescence resonance energy transfer (BRET) is a biophysical phenomenon describing a distance-dependent non-radiative energy transfer between a luciferase-luciferin and an acceptor chromophore similar to Fluorescence Resonance Energy Transfer (FRET) [1]. BRET usually occurs within close proximity (<10 nm) of the luminophore and fluorophore, which has been extensively exploited to monitor biomolecular dynamics, such as in the study of protein-protein interactions (PPIs) [2,3], molecular rearrangements [4,5], ligand-binding [6,7] and enzymatic assays [8,9]. Light emission as a consequence of BRET is initiated by an enzymatic reaction, where a luciferase catalyses the oxidation of a substrate to generate bioluminescence. Unlike FRET, BRET does not rely on external illumination, making it particularly well-suited for studying molecular dynamics in matrices containing autofluorescent molecules that are triggered by external excitation, such as in blood, cell cultures or *in vivo* applications, if using BRET acceptors with appropriate emission characteristics [10].

The rate at which energy transfer occurs is determined by a range of factors, such as the spectral overlap between donor emission and acceptor excitation, quantum yield of the donor,

* Corresponding author.
E-mail address: felix.weihs@csiro.au (F. Weihs).

https://doi.org/10.1016/j.acax.2020.100059

relative orientation between the transition dipole moments of the chromophores (κ) and their spatial separation.

The Förster distance (R_0) is the distance between the chromophores at which 50% of RET occurs. R_0 is a critical factor to consider before planning an interaction study as different experimental setups could favour longer or shorter Förster distances. PPI studies, for example, might benefit from shorter Förster distances as a larger R_0 distance could result in energy transfer signal even if the proteins of interest are close to each other but not interacting with each other. This is of interest in PPI analyses within confined subcellular compartments such as membranes. However, the analysis of molecular rearrangements in proteins such as G-protein coupled receptors (GPCRs) has been shown to benefit from large R_0's in certain circumstances. In one example, an internal loop and the C-terminus of a GPCR were tagged with RET components and upon ligand-binding, the induced conformational change resulted in a change in BRET efficiency [11]. Ideally, R_0 should match the distance between both tagged locations so that the dynamic conformational changes are transduced within the Förster working range ($R_0 \pm ½ R_0$), leading to improved sensitivities. Studies in which the distance between the tagged loci is > 6 nm, e.g. particular studies with GPCRs [11] and periplasmic binding proteins [12], have benefited from a large R_0.

Förster distances have been calculated, or experimentally determined, for a range of RET combinations and they can range from 3.17 nm between two fluorescent proteins (BFP-DsRED) [13] to 13 nm between two organic dyes incorporating a silver particle (Cy5-Cy5.5) [14]. R_0 can be calculated, assuming that the orientation factor κ^2 equals $^2/_3$ [15], and that the RET components are in fast isotropic motion. However, this assumption is not applicable to fluorescent proteins due to their size and fixed orientation [16]. We have previously experimentally determined the R_0 of a BRET^2 variant (RLuc8-GFP^2) as 8.15 nm [17], the largest Förster distance reported for any genetically encoded RET system to date. BRET^2 has been a highly useful analytical tool due to its large spectral separation of 115 nm, particularly where its larger R_0 is advantageous compared to other RET systems. However, BRET^2 exhibits some notable shortcomings: Its light output is low and is accompanied by a fast signal decay compared to other BRET alternatives [18]. In addition, its emission profile within the blue/green light electromagnetic spectrum is heavily subjected to light absorption in *in vivo* applications [19].

Recently developed BRET systems based on the NanoLuc luciferase [24,25] and the BRET^6 system [10] offer up to 300x brighter bioluminescence signals and extend the emission profile into the red spectrum. Specifically, NanoBRET, which utilises NanoLuc as the energy donor, has developed into one of the most popular BRET systems in recent years. R_0 has not been determined for either system. This study aimed to fill this knowledge gap and extend the palette of available BRET Förster distances to give researchers a better-informed choice on BRET systems.

In this study, the Förster distances of NanoBRET in combination with a range of acceptors and the Förster distance of BRET^6 are reported for the first time. This was achieved by experimentally determining R_0 values by separating donor and acceptor molecules using flexible peptide linkers of known lengths [21] to correlate observed BRET efficiencies with chromophore-to-chromophore distances. Förster curves were further corroborated by cloning Carbonic Anhydrase II, a protein with a resolved crystal structure and known terminus-to-terminus distance, in between two of the NanoBRET combinations.

2. Materials and methods

2.1. Cloning, expression and purification of BRET constructs

BRET-protein overexpression plasmids were constructed by cloning genes into pRSET (ThermoFisher Scientific) using standard techniques. His-tagged BRET proteins were expressed in *E. coli* BL21 (DE3) cells (New England Biolabs, USA) and purified from lysates using HisTrap HP 1 mL columns integrated into an ÄKTAxpress Fast Performance Liquid Chromatography system (GE Healthcare, Australia), dialysed against 50 mM Tris (pH 8), 50 mM NaCl at 4 °C, snap-frozen and stored at −80 °C. Their purity was analysed by SDS-PAGE (Fig. S1). HaloTag-containing purified proteins were labelled by incubating 100 nM protein stocks (diluted in phosphate buffered saline (PBS; 10 mM Na_2HPO_4, 1.8 mM KH_2PO_4, 137 mM NaCl, 2.7 mM KCl, pH 7.4)) containing 2 μM TMR or 0.4 μM NCT at 30 °C for 1 h before BRET analyses. For detailed experimental details see the supplementary information.

2.2. BRET measurements

All BRET analyses were performed in 100 μL total volumes containing a concentration of 10 nM BRET construct in PBS. BRET reactions were initiated by the addition of 5 μL Furimazine (FZ) (1:10 dilution in Nano-Glo® buffer, Promega) for NanoBRET or 5 μL Coelenterazine-h (CTZ-h; 100 μM in PBS containing 10%

Table 1
Förster distances (R_0) of BRET and FRET systems.

Resonance Energy Transfer type	Donor	Acceptor	Determination	R_0 (nm)	Working range (nm)	Reference
Bioluminescence Resonance Energy Transfer	NanoLuc	HaloTag (TMR)	experimental	6.15 ± 0.03	3.08–9.23	This work
	NanoLuc	HaloTag (NCT)	experimental	6.97 ± 0.03	3.49–10.46	This work
	NanoLuc	Venus	experimental	5.59 ± 0.04	2.80–8.39	This work
	NanoLuc	mCherry	experimental	5.43 ± 0.02	2.72–8.15	This work
	RLuc8.6	$TurboFP_{635}$	experimental	5.47 ± 0.01	2.74–8.21	This work
	RLuc8	GFP^2	experimental	8.15	4.08–12.23	[17]
	RLuc2	GFP^2	experimental	7.67	3.84–11.51	[17]
	RLuc	GFP^2	experimental	7.50	3.75–11.25	[20]
	RLuc	YFP	experimental	4.44	2.22–6.66	[20]
	RLuc2	Venus	experimental	5.68	2.84–8.52	[17]
	RLuc8	Venus	experimental	5.55	2.78–8.33	[17]
Fluorescence Resonance Energy Transfer	BFP	DsRED	calculated	3.17	1.59–4.76	[13]
	LSSmOrange	mKate2	calculated	7.0	3.5–10.5	[15]
	mAmetrine	tdTomato	calculated	6.6	3.3–9.9	[15]
	eCFP	eYFP	experimental	4.8	2.4–7.2	[21,20]
	CyOFP1	mCardinal	calculated	6.9	3.45–10.35	[15]
	$NaY_{0.78}F_4$:$Yb_{0.2}$,$Er_{0.02}$	QD (CdTe)	experimental	5.5	2.75–8.25	[22]
	Cy5	Cy5.5	experimental	8.3–13	4.15–12.45 to 6.5–19.5	[14]
	Si QDs	Si QDs	experimental	5–7.5	2.5–7.5 to 3.75–11.25	[23]

EtOH) for BRET^6, followed by immediately recording the BRET signal.

Dual emission BRET measurements and spectral scans were recorded with a CLARIOstar plate reader (BMG LabTech, Australia). Filter bandwidth selections and measurement details can be found in the supplementary information.

The mean value of 10 consecutive measurements, recorded with an integration time of 0.5 s, was used to calculate the BRET ratios (acceptor intensity divided by donor intensity).

2.3. Determination of Förster curves

Data analysis was carried out using GraphPad Prism (version 7 for Windows, GraphPad Software, San Diego, California, USA), MARS Data Analysis Software (BMG LabTech, Australia), RStudio (RStudio Inc, USA) and Office Excel. BRET efficiencies (E_{BRET}) were calculated using Eq. (1),

$$E_{BRET} = 1 - \left(\frac{I_{DA}}{I_D}\right) \quad (1)$$

where I_{DA} and I_D are the BRET ratios in the presence or absence of the RET acceptor, respectively. BRET efficiencies were then fitted to the Förster equation (Eq. (2)) using the GraphPad Prism non-linear fit function.

$$E_{BRET} = \frac{R_0^6}{R_0^6 + r_{BRET}{}^6} \quad (2)$$

The data point for a 20 nm donor-acceptor separation was determined by the 'simulate XY data function' in GraphPad Prism by integrating the experimentally determined R_0 into Eq. (2).

3. Results

3.1. Selected BRET combinations

We selected BRET^6 for our investigation, as it has been recently shown to be a sensitive backbone for protease detection in human plasma [8] and a good imaging tool in mice [10]. It comprises the red-shifted *Renilla* luciferase RLuc8.6, with the CTZ-h substrate, and the fluorescent protein TurboFP$_{635}$ (Katushka) [10]. NanoLuc has been extensively used in combination with the yellow fluorescent protein Venus [26,27] or HaloTag [6], a self-labelling enzyme that incorporates chloroalkene-functionalised fluorescent ligands [28]. As Venus exhibits an emission peak within the 'yellow' electromagnetic spectrum (530 nm), we alternatively incorporated a red-shifted fluorescent protein, mCherry, which has an emission peak at 610 nm in its place. For NanoBRET using HaloTag, RET from NanoLuc(FZ) to the two most commonly used HaloTag fluorescent ligands was investigated: Tetramethylrhodamine (TMR) and non-chloro TOM (NCT or NanoBRET 618) which have emission peaks at 585 nm and 618 nm, respectively.

3.2. Orientation dependence

To optimise the orientation between luciferase and acceptor, RLuc8.6 was cloned to the C-terminus of TurboFP635 separated by glycine/serine peptide linker repeats $(GGSGGS)_n$ (n = 1–9). Previous studies showed that *Renilla* luciferases exhibit enhanced RET efficiencies, if the C-terminus of RLuc remains unconstrained [29]. The optimal orientation of NanoLuc to fluorescent proteins or HaloTag was analysed by cloning NanoLuc to the N- or C-terminus of Venus, mCherry and HaloTag interposed with a single linker segment $(GGSGGS)_1$.

C-terminal and N-terminal NanoLuc-acceptor fusions were spectrally analysed to identify which orientation resulted in the largest BRET efficiency (Fig. 1a–d). Both fusions of NanoLuc with mCherry or Venus exhibited higher acceptor emission intensity to donor emission intensity if NanoLuc was fused to the C-terminus of the fluorescent protein (Fig. 1a and b). The BRET ratio decreased by 30% from 0.86 for a C-terminal NanoLuc fusion to 0.6 for an N-terminal fusion (Fig. 1f). Similarly, NanoLuc fused to the C-terminus of Venus exhibited a BRET ratio of 1.63 that decreased by 27% to 1.19 for an N-terminal NanoLuc fusion. For NanoBRET with HaloTag, BRET ratios increased from 0.31 for a C-terminal NanoLuc fused to HaloTag (TMR) by 459% to 1.40 for an N-terminally fused NanoLuc, whereas a 687% increase in BRET ratio from 0.09 to 0.59 was observed, when comparing a C-terminal NanoLuc to HaloTag (NCT) fusion with an N-terminal fusion (Fig. 1c,d,f). This effect is the opposite to NanoLuc-fluorescent protein fusions, as well as for RLuc-Fluorescent protein fusions, which could be due to a different relative orientation of the transition dipole moments between NanoLuc(FZ) to Venus/mCherry or NanoLuc(FZ) to HaloTag (TMR/NCT).

For all further experiments, fusions with NanoLuc at the C-terminus of Venus or mCherry and at the N-terminus of HaloTag were used. This was achieved by cloning $(GGSGGS)_n$ linker repeats in between BRET components.

3.3. BRET efficiencies

BRET ratios for all tested BRET combinations decreased with increasing flexible linker lengths (Table S1). Ratios were then translated into BRET efficiencies (eq. (1)) using a ratiometric approach as described previously [17].

BRET^6 exhibited a BRET efficiency of 83% with the shortest linker (FL_1), which decreased to 69% when the BRET components were separated by the FL_9 linker (Table S1). The NanoLuc-fluorescent protein combinations exhibited BRET efficiencies ranging from 87% (FL_1) to 83% (FL_9) for NanoLuc-Venus and BRET efficiencies ranging from 86% (FL_1) to 81% (FL_9) for NanoLuc-mCherry. BRET efficiencies observed for NanoLuc-HaloTag systems decreased from 93% (FL_1) to 87% (FL_9) with TMR as a ligand for HaloTag while the BRET efficiencies decreased from 96% (FL_1) to 94% (FL_9) using NCT as the ligand. NanoBRET efficiencies between NanoLuc(FZ) and HaloTag (TMR/NCT) are thus more efficient than those for BRET^6 or NanoLuc- FP combinations using the shortest peptide linker in the following order: NanoLuc(FZ) - HaloTag (NCT) > NanoLuc(FZ) - HaloTag (TMR) > NanoLuc(FZ) - Venus > NanoLuc(FZ) - mCherry > RLuc8.6 (CTZ-h) - TurboFP635.

3.4. BRET distances and experimental determination of Förster curves

To fit the observed BRET efficiencies with the distance between the BRET chromophores (r_{BRET}), it was assumed that all proteins exhibit a globular structure with a volume of ~0.74 cm^3/kg [30], with the chromophores sitting in the centre of the protein. Protein radii were calculated using Eq. (3).

$$Rd = 0.676\sqrt[3]{MW} \quad (3)$$

According to these calculations, the radius of RLuc8.6 was 2.23 nm and that of TurboFP635 was 2.01 nm. Combined with the known average lengths of the linker peptides [20], the estimated distances between both luminophores ranged from 4.15 ± 0.03 nm (TurboFP$_{635}$-FL$_1$-RLuc8.6) to 4.80 ± 0.05 nm (TurboFP635-FL$_9$-RLuc8.6) (Table S1). Fitting the BRET efficiencies against calculated distances using the Förster equation (Eq. (2)) gave a Förster distance

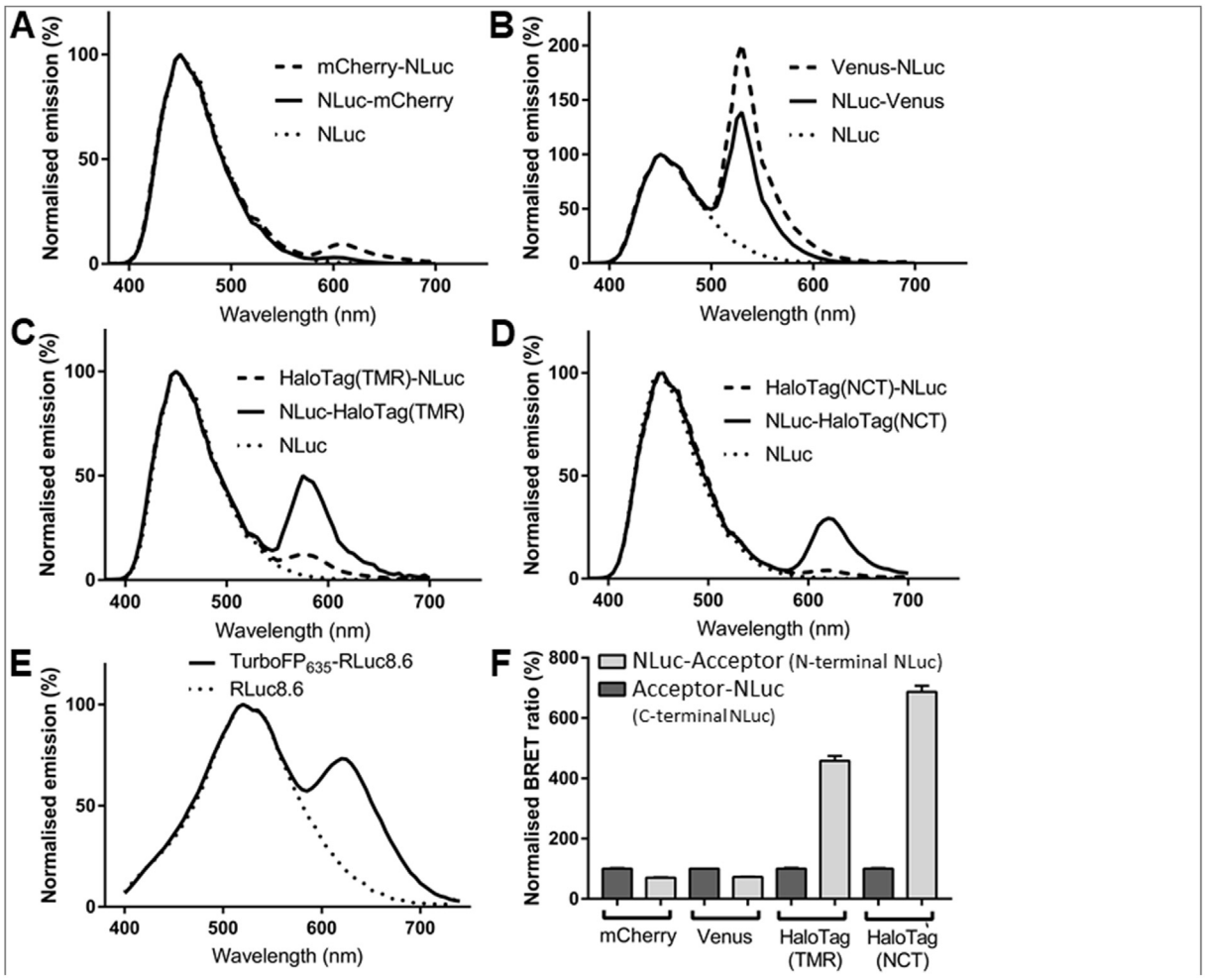

Fig. 1. Orientation dependence of the investigated BRET combinations.
A-D, Normalised bioluminescence spectra of NanoLuc (dotted line), C-terminal fusion of NanoLuc with acceptor protein (dashed line) and N-terminal fusion of NanoLuc with acceptor protein (solid line) using Furimazine as the luciferase substrate. **E**, Normalised bioluminescence spectra of RLuc8.6 (dotted line) and BRET^6 (solid line) using Coelenterazine-h as the luciferase substrate. All spectra were normalised to the luciferase peak intensity. **F**, Normalised BRET ratios of C- and N-terminal NanoLuc fusions with mCherry, Venus, HaloTag (TMR) and HaloTag (NCT). BRET ratios were normalised to the ratio of the C-terminal fusion, respectively.

of 5.47 ± 0.02 nm (95% confidence: 5.44–5.50 nm, R^2 = 0.993) (Fig. 2a).

The same procedure was applied to estimate the distances for the NanoBRET systems following the same assumptions as for BRET^6. HaloTag is a globular protein containing a ligand-binding cavity [31] (Fig. S2a). In a translational fusion of NanoLuc to the N-terminus of HaloTag (Fig. S2b), it appears that the chromophore-to-chromophore distance spans across the radii of both proteins. The radius of NanoLuc was thus to be calculated as 1.81 nm and that of HaloTag as 2.18 nm. These distances translate into r_{BRET} distances of 3.75 ± 0.03 nm (FL_1) to 4.40 ± 0.05 nm (FL_9) for Venus/mCherry-NanoLuc fusions and of 3.90 ± 0.03 nm (FL_1) to 4.55 ± 0.05 nm (FL_9) for NanoLuc-HaloTag. Fitting the r_{BRET} values against the BRET efficiencies demonstrated Förster distances of 5.43 ± 0.02 nm for mCherry-NanoLuc (95% confidence: 5.38–5.48 nm, R^2 = 0.992) and 5.59 ± 0.05 nm for Venus-NanoLuc (95% confidence: 5.50–5.69 nm, R^2 = 0.996), respectively (Fig. 2b, Table 1).

As the data points for NanoLuc-HaloTag lie at the top of the slope of the Förster curves, we decided to increase the distance between the BRET components to give a RET distance located within the dynamic part of the curve. Carbonic anhydrase 2 (CAII) was selected for this purpose, as its crystal structure is known [32] and its protein termini are located on opposite sides of the protein with an estimated C-to-N-terminus distance of 4.34 ± 0.17 nm (SI, Fig. S2c). This predicts a chromophore-to-chromophore distance of 8.24 ± 0.17 nm, which lies within the dynamic part of the Förster curve for the NanoLuc-HaloTag systems (Fig. 2c). BRET ratio analyses resulted in a BRET efficiency of 15% for NanoLuc-CAII-HaloTag using TMR as a ligand and of 29% using NCT as a ligand, respectively (Fig. 2c). Förster distances for NanoBRET were determined to be 6.17 nm using TMR as the HaloTag ligand (Figs. 2c) and 7.09 nm when NCT was used as the HaloTag ligand (Fig. 2c). R_0 of BRET^6 was therefore very similar to those seen for NanoBRET to Venus or mCherry. NanoBRET to HaloTag however, exhibited a larger Förster distance compared to any of the other systems evaluated in this study using either HaloTag ligand. This distance was largest when NCT was used.

3.5. Förster working distance ranges

Using RET as a molecular ruler is most powerful if the maximal dynamics of the probed system reflects the dynamic part of the Förster curve. This is the case if two tagged loci of a protein undergo conformational movements within the Förster working range

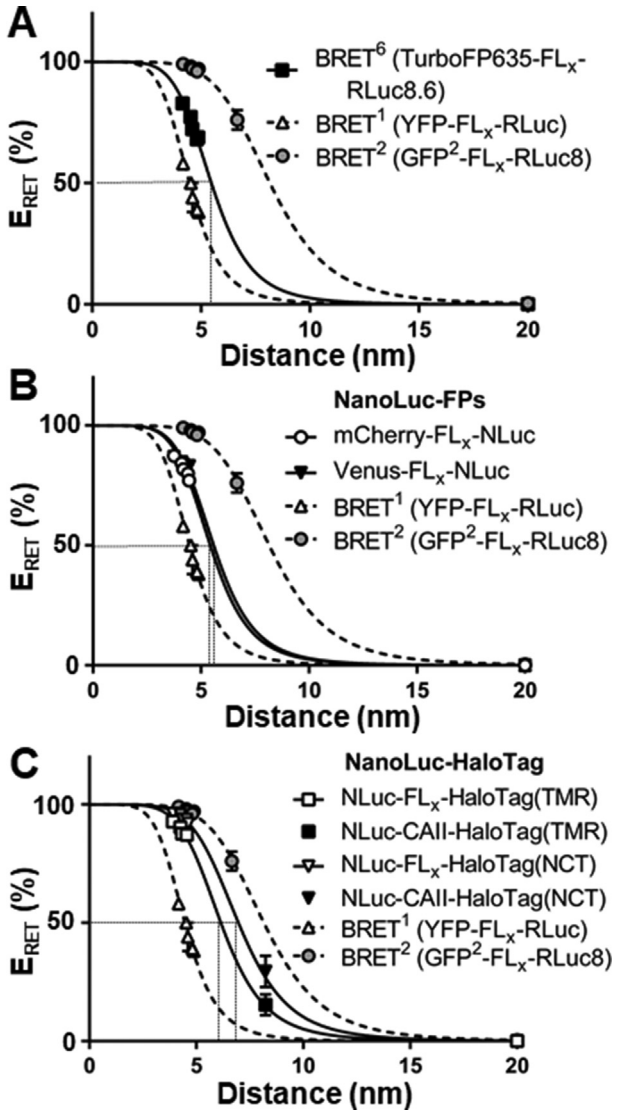

Fig. 2. RET efficiency dependent on the separation of donor and acceptor (in nm). Resonance energy transfer (RET) efficiency of BRET^6 (**A**), NanoLuc-fluorescent protein (FP) combinations (**B**) and NanoLuc-HaloTag combinations (**C**) were fitted against donor/acceptor separation with the Förster equation ($R > 0.975$). Förster curves of BRET^1 (eYFP-RLuc) and BRET^2 (GFP^2-RLuc8) were determined in a previous study [17,20] and are shown for comparison. The BRET efficiencies for NanoLuc-carbonic anhydrase 2 (CAII)-HaloTag (TMR/NCT) were plotted against 8.24 nm (**C**). Data are represented as mean ± standard deviation (n = 4). Dotted lines indicate the Förster distance corresponding to a BRET efficiency of 50%.

($R^0 \pm ½ R^0$). Smaller distances, where the Förster curve exhibits efficiencies >90–95%, will result in little to no reductions in the BRET ratio, while longer distances lie outside of the possible detection distance range. In this study, experimentally determined Förster distances reveal a working range of 2.74 nm–8.21 nm for BRET^6 (Fig. 3, Table 1), which is larger than that of the original BRET^1 system (RLuc-YFP), but shorter than that of the BRET^2 system [17]. NanoBRET with fluorescent proteins mCherry or Venus, exhibited working ranges of 2.72–8.15 nm and 2.80–8.39 nm, respectively, similar to that of BRET^6, while NanoBRET with HaloTag exhibited a working range of 3.08–9.23 nm (TMR) and 3.49–10.46 nm (NCT). Interestingly, the NanoBRET (NCT) working range enables reliable distance measurements at 10 nm. This was previously only achieved by three other genetically encoded RET

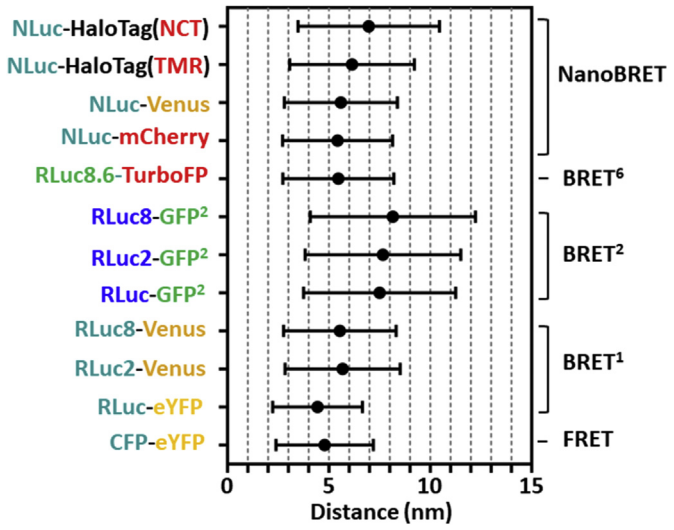

Fig. 3. Experimentally determined working distances of BRET and FRET
Working distance is defined as $0.5xR_0 - 1.5xR_0$. The filled circles indicate the Förster distance (R_0). Data of BRET^1, BRET^2 and FRET were determined previously [17,20].

systems, BRET^2 [17], LSSmOrange-mKate2 and CyOFP1-mCardinal [15] (Table 1).

4. Discussion

Förster distance is determined by the spectral overlap between donor emission and acceptor excitation, quantum yield of the donor and the relative transition dipole orientation factor. NanoLuc oxidising Furimazine exhibits a quantum yield of 5% [25], similar to that of *Renilla* luciferase-coelenterazine-h combinations [33], while RLuc8 catalysing the BRET^2 substrate coelenterazine 400a (DeepBlueC) exhibits a very low quantum yield of 0.12%. The differences in quantum yield are small and do not explain the larger Förster distances of NanoBRET and NanoLuc-FP combinations compared to the original BRET^1 system (RLuc-YFP) [20]. Apart from the quantum yield of BRET^2, the spectral overlap between NanoLuc(FZ) emission with the excitation spectra of the acceptors analysed in this study, demonstrates higher overlaps with Venus (48%) and TMR (49%) compared to NCT (19%) and mCherry (18%) (Fig. S3a). Hence, the amounts of spectral overlap do not correspond with the observed Förster distances. It is possible that the relative orientation between their dipole moments is a decisive factor here. This could be explained by a less fixed orientation of the HaloTag ligands, leading to efficient energy transfer and increased R_0 [16].

The BRET^6 Förster distance is similar to those determined previously for enhanced BRET^1 combinations (RLuc2-Venus/Rluc8-Venus) [17]. BRET^6 exhibits a slightly higher spectral overlap area (60%) than that of RLuc8-Venus (56%). However, its quantum yield is potentially lower, as previous work shows this to be 3.1% for RLuc8.6 catalysing CTZ compared to 6.9% for RLuc8(CTZ). The trade-off between lower quantum yield and higher spectral overlap could thus explain the similar Förster distances of BRET1 and BRET6.

A red-shifted NanoLuc variant-substrate combination (teLuc-DTZ), recently developed by Yeh et al. [34], could further enhance the Förster distance for NanoBRET, as teLuc(DTZ) exhibits a two-fold improved quantum yield of 10.8% over NanoLuc(FZ). This luciferase when combined with the fluorescent protein CyOFP1 is termed Antares2 [34]. Antares2 exhibits a high spectral overlap between donor emission and acceptor excitation profiles, which could lead to an even larger Förster distance than the NanoLuc-fluorescent protein combinations described in this study. Further

enhanced Förster distances for NanoBRET could also be achieved using ligands with increased excitation coefficients and higher overlap integrals compared to TMR and NCT [35].

While BRET^2 has historically been applied in the evaluation of GPCR receptor signalling [36], NanoBRET (NCT) could take over the niche of BRET^2 in the study of macromolecular interactions due to its large Förster distance of 6.97 nm, just under that of BRET^2. Unlike the shortcomings of BRET^2, NanoBRET (NCT) exhibits bright and sustained bioluminescence together with an excellent spectral separation of 158 nm. NanoBRET using TMR as a ligand might be of interest as a tool to measure conformational changes upon ligand-binding to GPCRs, as the distance between the third intracellular loop and the C-terminus in a β-2-adrenergic receptor averages 6.2 nm [37], close to the R_0 of NanoBRET (TMR).

Ultimately, the selection of RET Förster distance depends on the application. NanoLuc-fluorescent protein combinations and BRET^6 are bright and red-shifted alternatives to BRET^1 for protein-protein interaction studies, since their moderate Förster working ranges avoid bystander RET with colocalised proteins. NanoBRET with HaloTag, on the other hand, is more suitable for applications that benefit from a large R_0 including the analysis of multi-protein complexes and intramolecular measurements in large proteins.

CRediT authorship contribution statement

Felix Weihs: Conceptualization, Methodology, Investigation, Validation, Formal analysis, Visualization, Writing - review & editing. **Jian Wang:** Investigation. **Kevin D.G. Pfleger:** Conceptualization, Formal analysis, Writing - review & editing. **Helen Dacres:** Conceptualization, Methodology, Formal analysis, Writing - review & editing.

Declaration of competing interest

The authors declare that they have no known competing financial interests or personal relationships that could have appeared to influence the work reported in this paper.

Acknowledgments

We would like to thank Matthew Dennis and Andrea North for their helpful suggestions in the preparation of the manuscript. This study was supported by the CSIRO Probing Biosystems Future Science Platform (Australia). K.D.G.P. is funded by the Australian Research Council (ARC) Centre for Personalised Therapeutics Technologies (IC170100016) and has received funding through the ARC Linkage Program (LP160100857) in partnership with Promega (United States), BMG LabTech (Germany), Dimerix (Australia), the University of Nottingham (United Kingdom) and the University of Queensland (Australia).

Appendix A. Supplementary data

Supplementary data to this article can be found online at https://doi.org/10.1016/j.acax.2020.100059.

References

[1] T. Forster, *Zwischenmolekulare energiewanderung und fluoreszenz, Ann Phys-Berlin 2 (1948) 55–75.
[2] S. Dimri, S. Basu, A. De, Use of BRET to study protein-protein interactions in vitro and in vivo, Methods Mol. Biol. 1443 (2016) 57–78.
[3] K.D. Pfleger, K.A. Eidne, Illuminating insights into protein-protein interactions using bioluminescence resonance energy transfer (BRET), Nat. Methods 3 (2006) 165–174.
[4] H. Schihada, S. Vandenabeele, U. Zabel, M. Frank, M.J. Lohse, I. Maiellaro, A universal bioluminescence resonance energy transfer sensor design enables high-sensitivity screening of GPCR activation dynamics, Commun Biol 1 (2018) 105.
[5] E. Lima-Fernandes, S. Misticone, C. Boularan, J.S. Paradis, H. Enslen, P.P. Roux, M. Bouvier, G.S. Baillie, S. Marullo, M.G. Scott, A biosensor to monitor dynamic regulation and function of tumour suppressor PTEN in living cells, Nat. Commun. 5 (2014) 4431.
[6] C.W. White, E.K.M. Johnstone, H.B. See, K.D.G. Pfleger, NanoBRET ligand binding at a GPCR under endogenous promotion facilitated by CRISPR/Cas9 genome editing, Cell. Signal. 54 (2019) 27–34.
[7] L.A. Stoddart, E.K.M. Johnstone, A.J. Wheal, J. Goulding, M.B. Robers, T. Machleidt, K.V. Wood, S.J. Hill, K.D.G. Pfleger, Application of BRET to monitor ligand binding to GPCRs, Nat. Methods 12 (2015) 661–663.
[8] F. Weihs, A. Peh, H. Dacres, A red-shifted Bioluminescence Resonance Energy Transfer (BRET) biosensing system for rapid measurement of plasmin activity in human plasma, Anal. Chim. Acta 1102 (2020) 99–108.
[9] H. Dacres, M. Michie, S.C. Trowell, Comparison of enhanced bioluminescence energy transfer donors for protease biosensors, Anal. Biochem. 424 (2012) 206–210.
[10] A. Dragulescu-Andrasi, C.T. Chan, A. De, T.F. Massoud, S.S. Gambhir, Bioluminescence resonance energy transfer (BRET) imaging of protein-protein interactions within deep tissues of living subjects, Proc. Natl. Acad. Sci. U. S. A. 108 (2011) 12060–12065.
[11] H. Dacres, J. Wang, V. Leitch, I. Horne, A.R. Anderson, S.C. Trowell, Greatly enhanced detection of a volatile ligand at femtomolar levels using bioluminescence resonance energy transfer (BRET), Biosens. Bioelectron. 29 (2011) 119–124.
[12] H. Dacres, M. Michie, A. Anderson, S.C. Trowell, Advantages of substituting bioluminescence for fluorescence in a resonance energy transfer-based periplasmic binding protein biosensor, Biosens. Bioelectron. 41 (2013) 459–464.
[13] G.H. Patterson, D.W. Piston, B.G. Barisas, Forster distances between green fluorescent protein pairs, Anal. Biochem. 284 (2000) 438–440.
[14] J. Zhang, Y. Fu, J.R. Lakowicz, Enhanced forster resonance energy transfer (FRET) on single metal particle, J Phys Chem C Nanomater Interfaces 111 (2007) 50–56.
[15] B.T. Bajar, E.S. Wang, S. Zhang, M.Z. Lin, J. Chu, A guide to fluorescent protein FRET pairs, Sensors 16 (2016) 1488.
[16] S. Mueller, H. Galliardt, J. Schneider, B.G. Barisas, T. Seidel, Quantification of Forster resonance energy transfer by monitoring sensitized emission in living plant cells, Front. Plant Sci. 4 (2013).
[17] H. Dacres, M. Michie, J. Wang, K.D. Pfleger, S.C. Trowell, Effect of enhanced Renilla luciferase and fluorescent protein variants on the Forster distance of Bioluminescence resonance energy transfer (BRET), Biochem. Biophys. Res. Commun. 425 (2012) 625–629.
[18] F.F. Hamdan, M. Audet, P. Garneau, J. Pelletier, M. Bouvier, High-throughput screening of G protein-coupled receptor antagonists using a bioluminescence resonance energy transfer 1-based beta-arrestin2 recruitment assay, J. Biomol. Screen 10 (2005) 463–475.
[19] F. Weihs, H. Dacres, Red-shifted bioluminescence Resonance Energy Transfer: improved tools and materials for analytical in vivo approaches, Trac. Trends Anal. Chem. 116 (2019) 61–73.
[20] H. Dacres, J. Wang, M.M. Dumancic, S.C. Trowell, Experimental determination of the Forster distance for two commonly used bioluminescent resonance energy transfer pairs, Anal. Chem. 82 (2010) 432–435.
[21] T.H. Evers, E.M. van Dongen, A.C. Faesen, E.W. Meijer, M. Merkx, Quantitative understanding of the energy transfer between fluorescent proteins connected via flexible peptide linkers, Biochemistry 45 (2006) 13183–13192.
[22] S. Melle, O.G. Calderon, M. Laurenti, D. Mendez-Gonzalez, A. Egatz-Gomez, E. Lopez-Cabarcos, E. Cabrera-Granado, E. Diaz, J. Rubio-Retama, Forster resonance energy transfer distance dependence from upconverting nanoparticles to quantum dots, J. Phys. Chem. C 122 (2018) 18751–18758.
[23] J.H. Cao, H.J. Zhang, X.K. Liu, N. Zhou, X.D. Pi, D.S. Li, D.R. Yang, Plasmon-coupled forster resonance energy transfer between silicon quantum dots, J. Phys. Chem. C 123 (2019) 23604–23609.
[24] M.P. Hall, J. Unch, B.F. Binkowski, M.P. Valley, B.L. Butler, M.G. Wood, P. Otto, K. Zimmerman, G. Vidugiris, T. Machleidt, M.B. Robers, H.A. Benink, C.T. Eggers, M.R. Slater, P.L. Meisenheimer, D.H. Klaubert, F. Fan, L.P. Encell, K.V. Wood, Engineered luciferase reporter from a deep sea shrimp utilizing a novel imidazopyrazinone substrate, ACS Chem. Biol. 7 (2012) 1848–1857.
[25] T. Machleidt, C.C. Woodroofe, M.K. Schwinn, J. Mendez, M.B. Robers, K. Zimmerman, P. Otto, D.L. Daniels, T.A. Kirkland, K.V. Wood, NanoBRET–A novel BRET Platform for the analysis of protein-protein interactions, ACS Chem. Biol. 10 (2015) 1797–1804.
[26] K. Suzuki, T. Kimura, H. Shinoda, G. Bai, M.J. Daniels, Y. Arai, M. Nakano, T. Nagai, Five colour variants of bright luminescent protein for real-time multicolour bioimaging, Nat. Commun. 7 (2016) 13718.
[27] A. Tiulpakov, C.W. White, R.S. Abhayawardana, H.B. See, A.S. Chan, R.M. Seeber, J.I. Heng, I. Dedov, N.J. Pavlos, K.D. Pfleger, Mutations of vasopressin receptor 2 including novel L312S have differential effects on trafficking, Mol. Endocrinol. 30 (2016) 889–904.
[28] G.V. Los, L.P. Encell, M.G. McDougall, D.D. Hartzell, N. Karassina, C. Zimprich, M.G. Wood, R. Learish, R.F. Ohana, M. Urh, D. Simpson, J. Mendez, K. Zimmerman, P. Otto, G. Vidugiris, J. Zhu, A. Darzins, D.H. Klaubert, R.F. Bulleit, K.V. Wood, HaloTag: a novel protein labeling technology for cell imaging and protein analysis, ACS Chem. Biol. 3 (2008) 373–382.
[29] P. Molinari, I. Casella, T. Costa, Functional complementation of high-efficiency

resonance energy transfer: a new tool for the study of protein binding interactions in living cells, Biochem. J. 409 (2008) 251–261.
[30] I. Bahar, R. Jernigan, K.A. Dill, Protein Actions : Principles and Modeling, Taylor & Francis Group, New York, 2017. Garland Science.
[31] M.G. Kang, H. Lee, B.H. Kim, Y. Dunbayev, J.K. Seo, C. Lee, H.W. Rhee, Structure-guided synthesis of a protein-based fluorescent sensor for alkyl halides, Chem. Commun. 53 (2017) 9226–9229.
[32] B. Sjoblom, M. Polentarutti, K. Djinovic-Carugo, Structural study of X-ray induced activation of carbonic anhydrase, Proc. Natl. Acad. Sci. U. S. A. 106 (2009) 10609–10613.
[33] A.M. Loening, A. Dragulescu-Andrasi, S.S. Gambhir, A red-shifted Renilla luciferase for transient reporter-gene expression, Nat. Methods 7 (2010) 5–6.
[34] H.W. Yeh, O. Karmach, A. Ji, D. Carter, M.M. Martins-Green, H.W. Ai, Red-shifted luciferase-luciferin pairs for enhanced bioluminescence imaging, Nat. Methods 14 (2017) 971–974.
[35] O.M. Thirukkumaran, C.R. Wang, N.J. Asouzu, E. Fron, S. Rocha, J. Hofkens, L.D. Lavis, H. Mizuno, Improved HaloTag ligand enables BRET imaging with NanoLuc, Frontiers in Chemistry 7 (2020).
[36] J.H. Felce, A. MacRae, S.J. Davis, Constraints on GPCR heterodimerization revealed by the type-4 induced-association BRET assay, Biophys. J. 116 (2019) 31–41.
[37] S. Granier, S. Kim, A.M. Shafer, V.R.P. Ratnala, J.J. Fung, R.N. Zare, B. Kobilka, Structure and conformational changes in the C-terminal domain of the beta2-adrenoceptor: insights from fluorescence resonance energy transfer studies, J. Biol. Chem. 282 (2007) 13895–13905.